P1.15

A NEW LAGRANGIAN MODEL OF SEA ICE

R. W. Lindsay* and H. L. Stern
Polar Science Center, Applied Physics Laboratory
University of Washington, Seattle, Washington

1. INTRODUCTION

We have developed a new Lagrangian dynamic sea ice model for regional forecasting, process studies, data assimilation, and global climate forecasting. The model can be used to estimate the ice movement, deformation, thickness, and surface heat fluxes over the entire Arctic basin. A Lagrangian model can work alone or complement an Eulerian model. Advantages of a Lagrangian model include:

- Data assimilation procedures for ice trajectories determined from buoys or satellite tracking are accommodated more naturally and in the process provide a unique and valuable method of model evaluation
- Sea ice retains its identity as a material element for long periods of time and a model that recognizes this fact may have a better chance of realistically modeling ice behavior
- Cells can be added and dropped as needed, unlike an Eulerian model in which all cells must be retained regardless of the ice extent
- Slip lines in the ice motion are accommodated more naturally because there is no internal grid coordinate system to skew the results
- Ice from source regions, such as a particular shelf, can be marked and traced in a more accurate manner, even with a low-resolution model
- A Lagrangian model can change the spatial resolution as the geophysical situation requires. It can be low where there is little spatial variability and high where the spatial variability is large, such as at the ice edge, near shore-fast ice, or in regions of strong shear. A nested-grid Eulerian model may have less flexibility.

1.1. A review of Lagrangian models

The model presented here follows closely on the work of others. Flato (1993) describes a Lagrangian ice model that uses the particle-in-cell (PIC) method. This method solves the momentum equation on a relatively coarse, fixed, Eulerian grid. The velocity is then interpolated to a set of Lagrangian particles that are advected individually through the model domain. A trio of studies by Gutfraind and Savage (1997a, b, 1998) more closely resembles what we have done. They apply a numerical technique, which was first widely used in the astrophysics community, called Smoothed Particle Hydrodynamics (SPH) (Monaghan, 1988, 1992). No underlying Eulerian grid is used to determine the momentum balance. In this technique, the momentum equation is solved for individual point-mass particles. The strain rate, needed to determine the internal stress in the ice, is determined at particle positions by summing over the properties of neighboring particles. A third related approach is that of Pritchard et al. (1990). They define an adaptive grid for the Bering Sea that deforms such that the final line of grid cells stays with the ice edge in a semi-Lagrangian manner. The grid is not entirely Lagrangian in that the grid velocity is not matched to the ice velocity at all locations and some grid points remain fixed. Finally, Hopkins (1996) devised a dynamic model of sea ice consisting of convex polygons (floes) of multiyear ice with polygons of first-year ice in between. Driven by an imposed strain field, the model calculates the forces on each parcel of ice and moves them accordingly.

1.2. Smoothed Particle Hydrodynamics

The momentum equation for sea ice includes an internal stress-gradient term that is derived from the spatial gradients of the ice velocity, the strain rates. In an Eulerian model the strain rates are easily determined by centered differencing of adjacent cell velocities. With the Lagrangian model the cell locations change constantly and are distributed irregularly. We solve this problem through the formalism of Smoothed Particle Hydrodynamics (SPH). SPH has been used widely to solve the momentum equation in a variety of modeling problems. It was first developed to solve astrophysical problems (Lucy, 1977; Gingold and Monaghan, 1977) and has now been applied (references in Monaghan, 1992) to gas dynamics, stellar collisions, impacts, cloud collisions, disks and rings, jets, motion near black holes, super novae, and special and general relativity. It has also been used for cohesive granular flow (Oger and Savage, 1999), and for sea ice (Gutfraind and Savage, 1997a, b,

* *Corresponding author's address:* Ronald W. Lindsay, Polar Science Center, University of Washington, 1013 NE 40th St., Seattle WA 98105; e-mail: lindsay@apl.washington.edu

1998). Our development of the SPH formalism follows that of Gutfraind and Savage who used it to determine the motion of sea ice at a crooked coastline, a marginal ice zone, and through a constricted passage. Here we apply it to the entire Arctic Basin.

SPH determines the local average of a smooth field quantity *f(r)* as a weighted summation of the property at the locations of neighboring particles. The weighted sum is derived from an area integral with a kernel function *W* (Monaghan, 1988)

$$\langle f(\mathbf{r})\rangle = \int f(\mathbf{r}')W(\mathbf{r}-\mathbf{r}', L)\,d\mathbf{r}' \qquad (1)$$

so that the value at the location $\mathbf{r}_i$ is approximated as

$$\langle f(\mathbf{r}_i)\rangle \cong \sum_{k=1}^{N} f_k a_k W(|\mathbf{r}_i-\mathbf{r}_k|, L) \quad , \qquad (2)$$

where a_k is the area of particle k, and $|\mathbf{r}_i-\mathbf{r}_k|$ is the distance to the kth particle. The kernel W is a radially symmetric function with unit area

$$\int W(\mathbf{r}, L)\,d\mathbf{r} = 1\,, \qquad (3)$$

where L is a smoothing length. One of the most accurate kernels is the Gaussian (Monaghan, 1992), and this is the kernel used in the present model, but others can be used to good advantage. For any W, the limit for small L must be δ, the Dirac delta function.

The key aspect of SPH is that the gradients of any field, such as the ice velocity, are also expressed as a summation, not with the weighting function W but with its first derivative (Monaghan, 1988),

$$\langle \nabla f(\mathbf{r}_i)\rangle \cong \sum_{k=1}^{N} f_k a_k \nabla_i W(|\mathbf{r}_i-\mathbf{r}_k|, L) \quad , \qquad (4)$$

where ∇_i represents the gradient with respect to the coordinates of particle *i*. Equation (4) is the heart of SPH; the spatial derivatives of the velocity (the strain rates) are computed as weighted sums over neighboring cells. For example, the SPH formulation of one element of the strain rate tensor for particle *i* is (Gutfraind and Savage, 1997a)

$$\dot{\varepsilon}_{xx,\,i} = \sum_{k=1}^{N} a_k(u_k-u_i)\,\frac{\partial}{\partial x_i}W(|\mathbf{r}_i-\mathbf{r}_k|, L)\,, \qquad (5)$$

where $\frac{\partial}{\partial x_i}$ is the derivative with respect to the coordinates of particle *i*. The following section describes our implementation of Smoothed Particle Hydrodyamics.

2. THE LAGRANGIAN ICE MODEL

The model is based on a set of Lagrangian cells. The cells are considered as individual regions of ice in the dynamic model, and each cell has an associated position (*x,y),* velocity *(u,v),* ice compactness *A,* and mean ice thickness *h.* The area of the cells is computed each time step from a Voronoi tessellation of the entire basin. The Voronoi polygon of a point contains the region closer to that point than to any other point. The parameters describing the cells are assumed to vary smoothly in space. The cells are initially given positions in a square grid. Cells may be removed if they lose all their ice, or merged with a neighbor (averaging the positions, velocities, thickness, and compactness) if they move too close together. Cells may also be created when ice forms in a formerly ice-free region, either as a result of off-shore flow or from freezing in the fall.

This first implementation of the model, focused on ice dynamics, has just two ice classes, open water and ice, following Hibler (1979), and uses a seasonally dependent ice-growth rate determined from the ice-growth table of Thorndike et al. (1975). Future versions will have a full thickness distribution and ice growth and melt rates determined from a multilayer thermodynamic model solved on a low-resolution Eulerian grid. Table 1 lists various model parameters and their values for our standard runs.

Coastal cells. The coastal boundary condition is established by assuming the coast consists of fixed cells with very thick ice. The coastal cells have a spacing of 25 km and have an assumed area of 2500 km^2 and an assumed ice thickness of 10 m. The idea is that these stationary cells will impose local strain-rate estimates via the SPH procedure that will create the necessary convergence and shear to approximate the internal ice stress in the coastal regions. The coastal cells are used in the strain-rate determinations and in interpolating ice thickness values for internal stress estimates.

Stress gradients. The velocity gradients (strain rates) can be found for any location using the SPH gradient formalism (including the points with zero velocity for the coast). However the ice stress is not defined for these coastal points so the stress gradient is not defined for cells near the coast. This problem is overcome by determining the strain rates and stress at four points near each cell, 1/4 of the initial cell spacing in the positive and negative *x* and *y* directions. The ice thickness and concentration are interpolated to the four locations as well. Any of the four points near a coast will have both an increased ice thickness and a strain rate reflecting the presence of the coast. The stress is determined from the strain rate at each of the four points following a viscous plastic constitutive law. The normal and tangen-

tial forces on the cell due to internal ice stress are then determined from the gradient in the stress tensor by simple finite differences of the stress values at the four points.

Nearest neighbors. In principle the summations in (4) and (5) should include all of the cells in the model, because the integral in (1) covers the entire area. In practice, the cells more than one or two length scales away from the point of interest have little impact because of the Gaussian decay of the weighting function. In order to improve the numerical efficiency, the summation was performed only on the nearest neighbors of a cell. Experiments showed that as few as N_{neibs} = 20 were needed to produce good results. The nearest neighbors for each cell were determined once a day.

Time stepping. The momentum equations are integrated in time using the fifth-order Runge-Kutta-Fehlberg method with an adaptive time step, as in the Fortran code RKF45 (Fehlberg, 1969). It adjusts the integration step size dynamically to achieve the required level of accuracy. The variables in the integration are the two components of the positions of all the ice cells and the two components of their velocities, [*x, y, u, v*]. For these simulations the tolerance in the positions was set at 25 m and in the velocity at 0.0001 m/s. The model uses a full step size of 0.5 day. This full time step is divided dynamically into 100 to 2000 small steps for integrating the position and velocity. The area, ice concentration, and mean ice thickness are also determined each small time step from the computed divergence. Typical step sizes are 100 to 1000 seconds and each small step requires six evaluations of the time derivatives d [*x, y, u, v*] / d*t*.

Velocity smoothing. In order to maintain numerical stability in the model near the boundaries we found it necessary to apply an SPH smooth to the velocity once each full time step. A smoothing length of 100 km was used. Because the smoothing includes the stationary coastal points, the speed of the cells near the coast is reduced in the process. The thickness and compactness are also smoothed to insure smooth fields, however the coastal points are not included for these variables.

Changes in the thickness and the compactness are computed following the procedures outlined in Hibler (1979). These equations are based on the divergence computed from the SPH-determined strain rates and on the ice growth rates for open water and for the thick ice. The ice growth table of Thorndike et al. (1975) provides the seasonal and thickness-dependent growth rates.

Forcings. The geostrophic wind is derived from the International Arctic Buoy Program (IABP) pressure fields. The monthly mean ocean currents are obtained from the output of an Eulerian fully coupled ice/ocean model (Zhang and Rothrock, 2000) with a grid cell size of 40 km. The currents are the climatological mean for the period 1979 to 1993. The winds and currents are linearly interpolated to cell locations. The initial mean ice thickness was taken from the mean ice thickness of the Eulerian model for the January of the initial year of a simulation.

3. MODEL RESULTS

Two samples of the model output are shown in Figures 1 and 2. Figure 1 shows the trajectories of all of the cells over a 10-day period with the color of the trajectories coded for the ice thickness. Strong variations in the shapes of the trajectories are seen from one region to another, yet locally the trajectories show a great deal of coherence, reflecting the imposed smoothness of the velocity field. The ice is almost stopped north of Greenland as a result of the internal ice stress in the thick ice found in this region. The ice is thickest near the Canadian archipelago, reflecting the initial ice thickness field. The model trajectories show moderately good correspondence with the buoy trajectories. In Fig. 2 the trajectories are shown for a 30-day period and the mean model ice velocity is interpolated to a regular grid.

Validation and sensitivity tests. A series of sensitivity tests were run to determine the best value to use for some of the model parameters with the buoy velocities providing the validation data. The test period was the year 1998, with the initial conditions provided by a one-year integration through 1997. Comparisons were made of the daily buoy velocity with the daily averaged model velocity interpolated to the buoy positions using the SPH interpolation procedure with a length scale of 100 km.

The mean speeds, the RMS vector difference in the velocities, the turning angles, and the vector correlations of the velocities were determined. The RMS difference is found from the magnitudes of the vector differences between the model and the buoy. In order to account for spatial and temporal variability in the regression coefficients, we have followed Thomas (1999) and binned the observations into a 160-km grid and one-month intervals. Velocities from grid squares and months with 10 or more buoy observations are used to determine a squared correlation coefficient. The median values of R^2 for all such fits are reported for each run of the sensitivity studies.

The parameters examined fall into two groups. One group consists of model numerical parameters (Table 2) and includes the length scale for the SPH strain-rate calculations, the number of neighbors included in the SPH calculations, the velocity tolerance, and the smoothing

length scale. The second group consists of physical parameters (Table 3) and includes the air drag coefficient, the air stress turning angle, the ice strength, and the yield ellipse aspect ratio.

Numerical parameters. The numerical-parameters sensitivity tests show that the simulations are not very sensitive to the values of the parameters. RMS differences range only between 0.061 and 0.064 m s^{-1} and the squared correlation coefficient range only from 0.626 to 0.638. The speed bias and the turning angle bias also do not change significantly. A larger length scale improves the correlation slightly but can smooth the velocity field excessively if it is too large. The model-buoy comparison is also surprisingly insensitive to the number of nearest neighbors used to determine the strain rates or to the velocity tolerance used to guide the adaptive time stepping. The time stepping is largely controlled by cells where the accelerations are large and these cells are typically located very near the coasts, where few buoys are deployed. More accurate solutions near the coasts (obtained with reduced error tolerances in the adaptive time stepping) are not reflected in improved performance statistics measured at the buoys, which are found mostly in the interior. The velocity smoothing scale also does not help the performance statistics. However if no smoothing is used, time series plots of the velocity of individual cells occasionally indicate unrealistic oscillatory behavior. The SPH interpolation procedure for estimating the model velocity at the locations of the buoys effectively smooths these oscillations among adjacent cells and the interpolated model velocity matches the buoy velocities quite well. However to avoid these oscillatory instabilities we think it best to include a small amount of smoothing of the velocity fields so as to insure that the assumption of a smoothly varying velocity field is accurate.

Physical parameters. The sensitivity tests for the physical parameters show that the magnitude of the speed bias is most sensitive to the air drag coefficient and is at a minimum (2.4%) for C_A = 0.0012. The angle bias is most sensitive, of course, to α, the turning angle for the wind stress. Because of the free parameters in the linear model used to compute the correlation, the correlation is insensitive to changes in either of these two parameters. The ice strength P^* and the aspect ratio of the yield ellipse have a limited impact on the velocity comparisons over the ranges tested. However the speed bias is reduced as the ice strength is increased. Perhaps most surprising in these tests is the insensitivity of the model simulations to changes in the key parameters. The model speed bias and turning angle bias respond as expected, but the RMS differences and the correlations do not change greatly within the testing range of the parameters.

The RMS differences and the correlation values for the Lagrangian model are comparable to those obtained with a state-of-the-art Eulerian ice-ocean model. Zhang *et al.* (2003) found the RMS differences between the ice velocity and the buoy velocities to be 0.070 m s^{-1} in both winter and summer over a five-year period and the correlation coefficients to be R = 0.66 in winter and R = 0.74 in summer. Our values for a one-year comparison show RMS differences to be 0.062 m s^{-1} for the standard case and the correlation coefficient for the year to be R =0.79.

4. SUMMARY AND CONCLUSIONS

The Lagrangian model presented here offers a new way to think about ice dynamics and ice processes. Instead of dividing the world into squares and attempting to keep track of the net flux of ice or momentum into and out of the squares (the classic Eulerian model), we attempt to follow the evolution of particular parcels of ice and model explicitly the forces that impinge on the parcel and the resulting parcel velocities and trajectories. This is a different approach and has required some innovation. In constructing an entirely new model we have become more aware than ever of the creative efforts needed to meld the physical laws of nature with a model framework that is logically and numerically tractable. By necessity, compromises were made, and those presented here are undoubtedly not the last word on the formulation of a Lagrangian dynamic sea ice model.

The most important attribute of the model is that it represents the ice pack with a set of mobile ice cells, each of which is characterized by position, velocity, mean thickness, and compactness. The velocity, thickness, and compactness are thought to vary smoothly in space. The equations of motion that are solved for each cell include terms for the water and air stresses, the Coriolis force, and internal ice stress gradients. The ice stress gradients are found from a viscous plastic rheology with an elliptic yield curve. The strain rates are found from a weighted sum of the velocities of 20 neighboring cells using the formalism of Smoothed Particle Hydrodynamics. Ice growth and melt rates are determined from a lookup table that depends on season and thickness.

The ice motion in the Arctic Ocean is well correlated with the geostrophic wind speed (Thorndike and Colony, 1982; Thomas, 1999). Thomas (1999) found that the median vector correlation of the geostrophic wind with the ice motion (as measured by buoys) is R^2 = 0.71 in the winter and 0.73 in the summer and fall. His analysis was for the 15-year period from 1979 through 1993 and he had removed the spatial and seasonal variability of

the linear relation by binning the data into 160-km squares for each month of the year. He also found that the RMS error of eight different formulations of a standard Eulerian model was larger than that found from the linear least-squares model. He found that for the Arctic Ocean the buoy mean field had an error of 0.085 m s^{-1} (the standard deviation), the linear model an error of 0.052 m s^{-1}, and the Eulerian model errors ranged from 0.061 to 0.089 m s^{-1}.

We compared the buoy, wind, and model velocities with separate fits for each 160-km square grid cell and for each month. The median values of R^2 and the errors in the fit were examined. The geostrophic wind for the five-year simulation is slightly better correlated (R^2 = 0.70) with the buoy velocities than the model is (R^2 = 0.68). The model velocities are more correlated with the geostrophic wind (R^2 = 0.88) than the buoys' are, in part because any error in the wind field is also reflected in the model response. The RMS difference between the model velocity and the buoy velocity is 0.065 m s^{-1}, much more than that of the linear model, 0.042 m s^{-1}. The fact that the model ice velocity error is larger than that of the best-fit least-squares model is not too surprising, because the best-fit model has the luxury of choosing a different set of coefficients for every location and month, coefficients that minimize the error by design.

The model performs stably with the adaptive time stepping procedure, which changes the size of the integration step size in order to keep the integration error below a set tolerance. This procedure allows the model to take as few as 200 or as many as 5000 steps in a half-day period. The model errors are not very sensitive to large changes in both numerical and physical model parameters.

Future work. This is a new ice dynamics model that can be refined before it is widely applied. The coastal boundary force could be modified to better allow for the possibility of fast ice. This would entail the formulation of a coastal force that allows for tensile strength. The number density could vary spatially by defining regions where the initial cell separation is smaller than found in the bulk of the basin, places of special interest such as in constricted regions, in shelf regions, or in marginal ice zones. The length scale is currently constant but it could be made to vary depending on the number density of the cells so that better spatial resolution of the velocity field could be obtained in regions with a high density of cells.

The thermodynamic growth and melt rates could be modeled using air temperature, wind speed, and short- and longwave radiative flux fields. The focus of this first study is on the Lagrangian dynamic model, so the thermodynamics have been subsumed into a simple season- and thickness-dependent ice-growth table. Along with the thermodynamics, a more physically realistic ridging and redistribution model could be included. The pack-ice model of Lindsay (2003) includes both a thermodynamic and an ice redistribution model and is designed to be used in a Lagrangian context.

Data assimilation. Finally, one of the prime motivations for designing this model has been to assimilate integral Lagrangian measures of the ice motion, such as from buoys or from the Radarsat Geophysical Processor System (RGPS) (Kwok, 1998). The RGPS provides measures of the ice motion for a large number of points with temporal intervals of 1 to 10 days. The cells of our Lagrangian model could be associated with particular RGPS trajectories. The model would provide the velocity estimates for intermediate times between the RGPS observations so that the velocity and deformation fields measured by the RGPS might be translated into regularly gridded fields, more easily used for Eulerian model validation or assimilation. Other potential applications of a model such as this are for long-range trajectory analysis (such as of ice production regions or for entrained-minerals tracing experiments), ice mixing (horizontal diffusion) studies, stress propagation analysis, ice rheology studies, or marginal ice zone prediction.

Animations of the model results may be found at the web site psc.apl.washington.edu/lindsay. An extended version of this paper has been submitted to the *Journal of Physical Oceanography* (Lindsay and Stern, 2003)

Acknowledgements

The buoy data were obtained from Ignatius Rigor of the International Arctic Buoy Program. The geostrophic winds, ocean currents, and initial ice thickness values were obtained from Jinlun Zhang of the Polar Science Center. This work was supported by the NASA Cryospheric Sciences Program, Grant NAG5-10621.

References

Fehlberg, E., 1969: Low-order classical Runge-Kutta formulas with stepsize control and their application to some heat transfer problems. NASA, Marshall Space Flight Center, Huntsville, AL, July 1969, NASA-TR-R-315, 46 pp.

Flato, G.M., 1993: A particle-in-cell sea ice model. *Atmos.-Oceans*, 31, 339–358

Gingold, R. A. and J. J. Monaghan, 1977: Smoothed particle hydrodynamics: Theory and applications to non-spherical stars. *Mon. Not. R. Astron. Soc.*, 171, 375–381.

Gutfraind, R. and S. B. Savage, 1997a: Smoothed particle hydrodynamics for the simulation of bro-

ken-ice fields: Mohr-Coulomb-type rheology and frictional boundary conditions. *J. Computational Physics*, 134, 203–215.

Gutfraind, R. and S. B. Savage, 1997b: Marginal ice zone rheology: Comparison of results from continuum-plastic models and discrete-particle simulations. *J. Geophys. Res.* 102(C6), 12,647–12,661

Gutfraind, R. and S. B. Savage, 1998: Flow of fractured ice through wedge-shaped channels: smoothed particle hydrodynamics and discrete-element simulations. *Mechanics of Materials*, 29, 1–17

Hibler, W. D., 1979: A dynamic thermodynamic sea ice model. *J. Phys. Oceanog.*, 9, 817–846.

Hopkins, M. A., 1996: On the mesoscale interaction of lead ice and floes, *J. Geophys. Res.*, 101, 18315-18326.

Kwok, R., 1998: The RADARSAT Geophysical Processing System. *Analysis of SAR Data of the Polar Oceans,* edited by C. Tsatsoulis and R. Kwok, Springer-Verlag, Berlin, 235–257.

Lindsay, R. W., 2003: Changes in the modeled ice thickness distributions near the SHEBA drifting ice camp. *J. Geophys. Res.*, in press, 10.1029/2001JC000805.

Lindsay, R. W. and H. L. Stern, 2003: A new Lagrangian model of Arctic sea ice, *J. Phys. Oceanog.*, submitted.

Lucy, L. B., 1977: A numerical approach to the testing of the fission hypothesis. *Astron. J.*, 82, 1013–1024.

Monaghan, J. J., 1988: An introduction to SPH. *Comput. Phys. Commun*. 48, 259–268.

Monaghan, J. J., 1992: Smoothed particle hydrodynamics. *Ann. Rev. Astron. Astrophys*. 30, 543–574.

Oger, L. and S. B. Savage, 1999: Smoothed particle hydrodynamics for cohesive grains. *Computer-Methods in Applied Mechanics and Engineering*. 180, 169–183.

Pritchard, R. S., A. C. Mueller, D. J. Hanzlick, and Y. S. Yang, 1990: Forecasting Bering Sea ice edge behavior. *J. Geophys. Res.*, 95, 775–788.

Thomas, D., 1999: The quality of sea ice velocity estimates. J. Geophys. Res., 104, 13,627-13,652.

Thorndike, A. S., D. A. Rothrock, G. A. Maykut, and R. Colony, 1975: The thickness distribution of sea ice. *J. Geophys. Res.*, 80, 4501–4513.

Thorndike, A. S. and R. Colony, 1982: Sea ice motion in response to geostrophic winds. J. Geophys. Res., 87(C8), 5845-5852.

Zhang, J., and D.A. Rothrock, 2000: Modeling arctic sea ice with an efficient plastic solution. *J. Geophys. Res.*, 105, 3325–3338.

Zhang, J., D. Thomas, D. A. Rothrock, R. W. Lindsay, Y. Yu, and R. Kwok, 2003: Assimilation of ice motion observations and comparisons with submarine ice thickness data. J. Geophys. Res., in press.

Table 1. Model Parameters, Standard Case

Parameter	Symbol	Value
Initial cell spacing	Δx	100 km
Coastal points spacing	Δx_{coast}	25 km
Number of Neighbors	N_{neibs}	20
SPH length scale	L	150 km
Smoothing scale	L_{smth}	100 km
Geostrophic wind drag coefficient	C_g	0.0012
Current drag coefficient	C_w	0.055
Wind stress turning angle	α	30°
Water stress turning angle	β	25°
New ice thickness	h_0	0.1 m
Coastal force length scale	L_{coast}	25 km
Coastal force strength	F_{coast}	0.1 N m^{-2}
Ice strength constant	P*	5000 N m^{-2}
Yield ellipse aspect ratio	e	2
Full time step	Δt	0.5 day
Position tolerance	e_x	25 m
Velocity tolerance	e_u	0.0001 m s^{-1}

Table 2. Sensitivity studies of model velocities compared to buoy velocities, numerical parameters

Parameter	Standard value	Adjusted values	Mean speed bias (fraction of mean)	Mean angle bias (deg)	RMS difference ($m\ s^{-1}$)	R^2
Std. Case			0.021	2.9	0.062	0.637
L (km)	150	100	0.042	2.6	0.061	0.628
		300	0.051	3.0	0.063	0.632
N_{neibs}	20	10	0.046	2.1	0.064	0.631
		30	0.038	2.7	0.063	0.632
e_u ($m\ s^{-1}$)	0.0001	0.001	0.021	1.9	0.064	0.629
		0.0005	0.023	2.7	0.064	0.636
L_{smth} (km)	100	none	0.046	4.9	0.064	0.626
		200	0.005	3.0	0.062	0.636

Table 3. Sensitivity studies of model velocities compared to buoy velocities, physical parameters

Parameter	Standard value	Adjusted values	Mean speed bias (fraction of mean)	Mean angle bias (deg)	RMS difference ($m\ s^{-1}$)	R^2
Std. Case			0.021	2.9	0.062	0.637
C_g	0.0012	0.0011	-0.036	3.0	0.062	0.640
		0.0013	0.079	3.5	0.064	0.633
α	30	20	0.026	-7.0	0.063	0.637
		40	0.039	14.3	0.066	0.630
P^*	5000	2500	0.046	1.6	0.062	0.632
		10000	-0.094	6.2	0.061	0.607
e	2	1	-0.013	3.6	0.061	0.615
		4	0.034	2.0	0.062	0.638

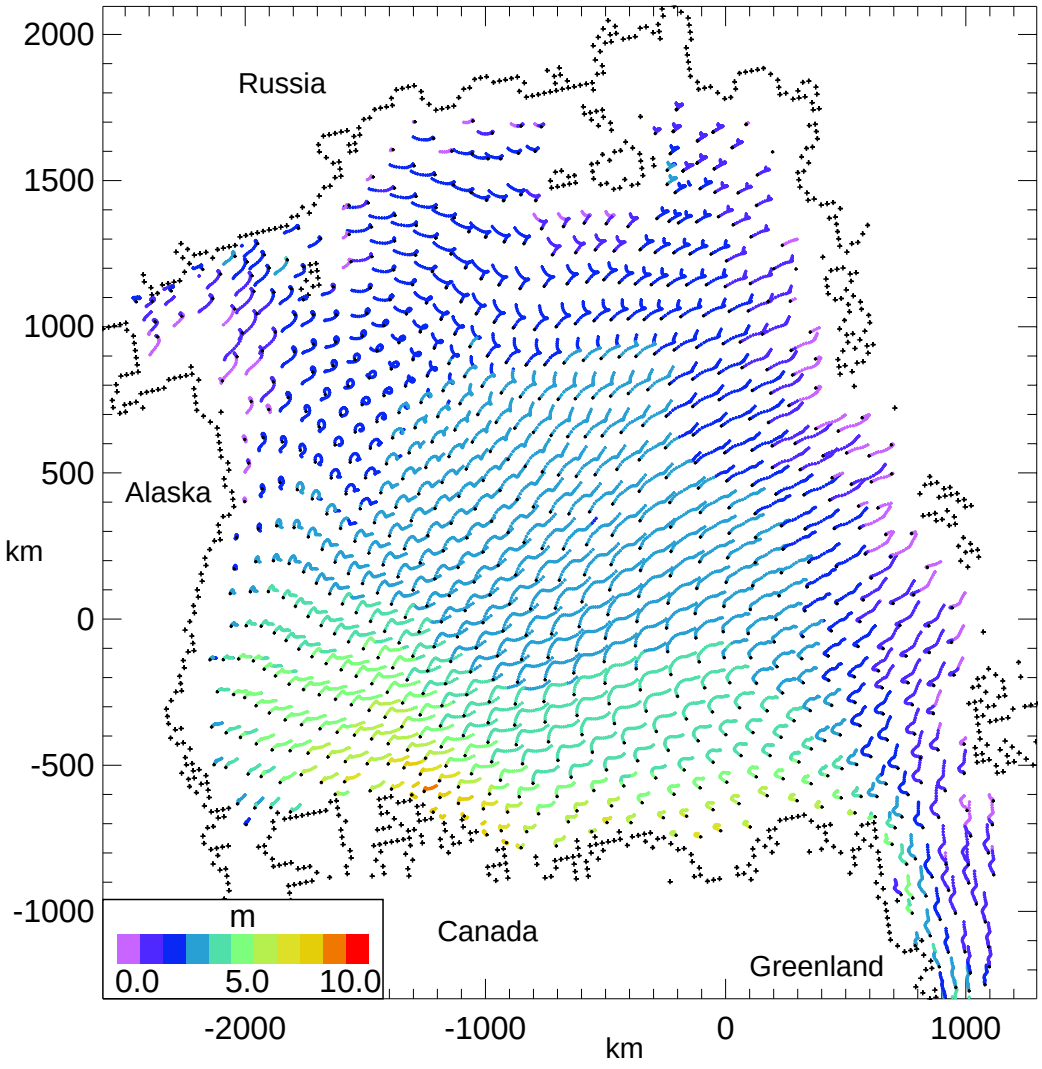

Fig. 1. Ten-day trajectories of all cells in the Arctic Basin from March 1997. The simulated thickness is color coded. A black dot marks the end of each trajectory.

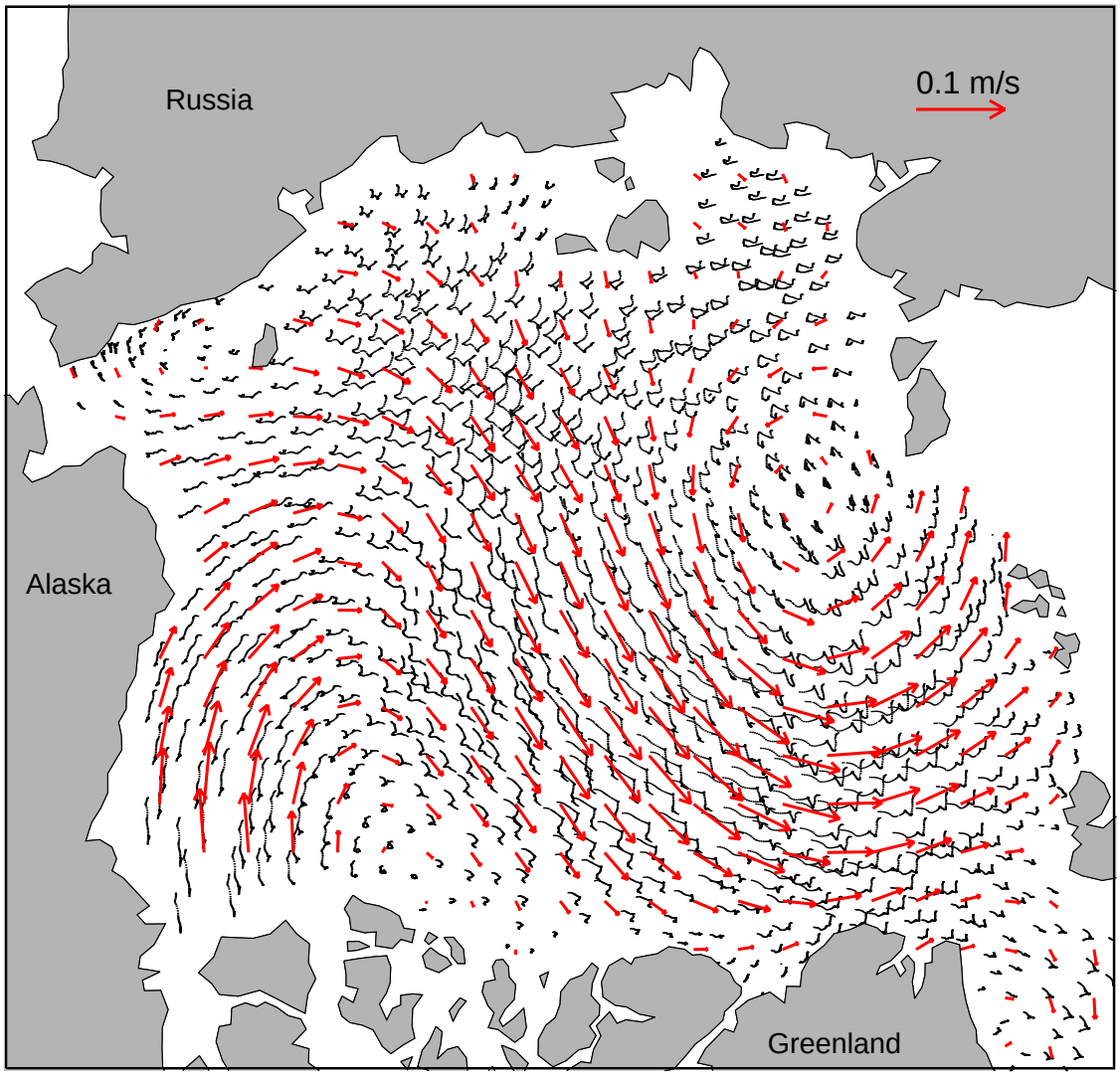

Fig. 2. Thirty-day model trajectories from June 1998. The mean thirty-day velocity field from the model, interpolated to a regular grid, is shown with red vectors.